Multiple chiral doublet candidate nucleus ^{105}Rh in a relativistic mean-field approach

Jian Li (李剑) and S. Q. Zhang (张双全)
School of Physics, State Key Laboratory of Nuclear Physics and Technology, Peking University, Beijing 100871, China

J. Meng (孟杰)*
School of Physics and Nuclear Energy Engineering, Beihang University, Beijing 100191, China,
School of Physics, State Key Laboratory of Nuclear Physics and Technology, Peking University, Beijing 100871, China and
Department of Physics, University of Stellenbosch, Stellenbosch, South Africa
(Received 7 January 2011; published 10 March 2011)

Following the reports of two pairs of chiral doublet bands observed in ^{105}Rh, the adiabatic and configuration-fixed constrained triaxial relativistic mean-field calculations are performed to investigate their triaxial deformations with the corresponding configuration and the possible multiple chiral doublet (MχD) phenomenon. The existence of the MχD phenomenon in ^{105}Rh is highly expected.

DOI: 10.1103/PhysRevC.83.037301 PACS number(s): 21.10.Dr, 21.60.Jz, 21.30.Fe, 27.60.+j

Chirality is a topic of general interest in the natural sciences, such as chemistry, biology, and physics. The occurrence of chirality in atomic nuclear structures was suggested for triaxially deformed nuclei in 1997 [1], and the predicted patterns of spectra exhibiting chirality, chiral doublet bands, were experimentally observed in 2001 [2]. In addition to the triaxial deformation, the configuration with high-j valence particle(s) and valence hole(s) is also essential for chirality in nuclei. Up to now, candidate chiral doublet bands have been proposed in a number of odd-odd, odd-A, or even-even nuclei in the $A \sim 100$, 130, 190 mass regions; for a review, see, e.g., Refs. [3,4].

With respect to theory, chiral doublet bands were first investigated in the one-particle-one-hole-rotor model (PRM) and the corresponding tilted axis cranking (TAC) approximation [1]. Later, numerous efforts were devoted to developing TAC [5–7] and PRM models [8–12] to describe chiral rotation in atomic nuclei.

Relativistic mean-field (RMF) theory has received wide attention due to its massive success in describing nuclear global properties and exotic phenomena [13–15]. In order to describe the nuclear rotation phenomena, the cranked RMF theory in the context of principal-axis rotation [16,17] as well as three-dimensional rotation [18] was developed. However, due to numerical complexity, it was restricted to two-dimensional studies only, i.e., the magnetic rotation [18,19].

Based on the adiabatic and configuration-fixed constrained triaxial RMF calculation, triaxial shape coexistence with high-j proton-hole and neutron-particle configurations is found in ^{106}Rh, which suggests the existence of a new phenomenon, the multiple chiral doublet (MχD) [20]. This prediction also holds true for other rhodium isotopes, ^{104,106,108,110}Rh [21]. In particular, the prediction of the MχD in ^{106}Rh remains even with the time-odd fields included [22].

Recently, two pairs of chiral doublet bands have been observed in ^{105}Rh with three-quasiparticle configurations, $\pi g_{9/2} \otimes \nu h_{11/2}(g_{7/2}, d_{5/2})$ [23] and $\pi g_{9/2} \otimes \nu h^2_{11/2}$ [24]. It is interesting to verify whether these observations are the predicted MχD or not in the configuration-fixed constrained triaxial RMF approach. As in Ref. [22], the time-odd fields are included.

The starting point of the RMF theory is the standard effective Lagrangian density constructed with the degrees of freedom associated with the nucleon field ψ, two isoscalar meson fields σ and ω_μ, the isovector meson field $\boldsymbol{\rho}_\mu$, and the photon field A_μ [13–15]. Under "mean-field" and "no-sea" approximations, one can derive the corresponding energy density functional, from which one finds immediately the equation of motion for a single-nucleon orbital $\psi_i(\mathbf{r})$ by variational principle,

$$\{\alpha \cdot [\mathbf{p} - \mathbf{V}(\mathbf{r})] + \beta M^*(\mathbf{r}) + V_0(\mathbf{r})\}\psi_i(\mathbf{r}) = \epsilon_i \psi_i(\mathbf{r}), \quad (1)$$

where $M^*(\mathbf{r}) \equiv M + g_\sigma \sigma(\mathbf{r})$, M is the mass of bare nucleon, $V_0(\mathbf{r})$ is the time-like component of vector potential, and $\mathbf{V}(\mathbf{r})$ are the space-like components of vector fields. The details of the solution of Dirac equation (1) with time-odd fields can be found in Refs. [25,26].

In the configuration-fixed constrained calculation, the same configuration is guaranteed during the procedure of constraint calculation with the help of "parallel-transport" [27]. In addition to the β^2-constrained calculation [20], the constraints on the axial and triaxial mass quadrupole moments are also performed to obtain the potential energy surfaces in the two-dimensional $\beta - \gamma$ plane [28].

In the present calculations, each Dirac spinor $\psi_i(\mathbf{r})$ is expanded in terms of a set of three-dimensional harmonic oscillator (HO) bases in Cartesian coordinates with 12 major shells and meson fields with 10 major shells. The pairing correlations are quenched by the unpaired valence nucleons in ^{105}Rh and thus neglected here. The effective interaction parameter set PK1 [29] is applied. The center-of-mass (c.m.) correction [29,30] is taken into account by

$$E^{\text{mic.}}_{\text{c.m.}} = -\frac{1}{2MA}\langle \hat{\mathbf{P}}^2_{\text{c.m.}} \rangle, \quad (2)$$

*mengj@pku.edu.cn

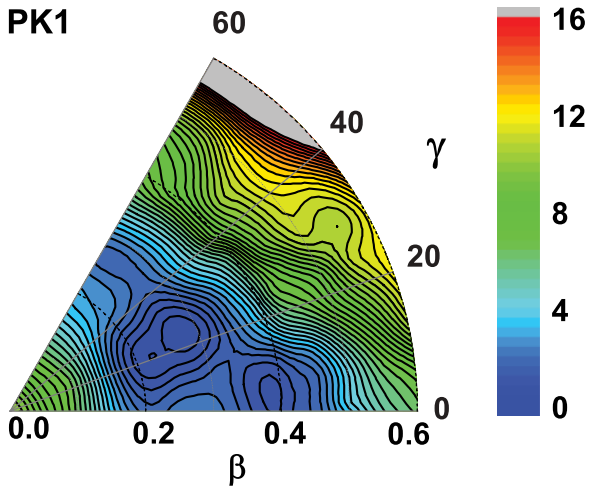

FIG. 1. (Color online) Contour plots of potential energy surface in the β-γ plane ($0 \leqslant \gamma \leqslant 60^\circ$) for ^{105}Rh in constrained triaxial RMF calculations with effective interaction PK1 [29]. All energies are normalized with respect to the binding energy of the absolute minimum (in MeV). The energy separation between contour lines is 0.4 MeV.

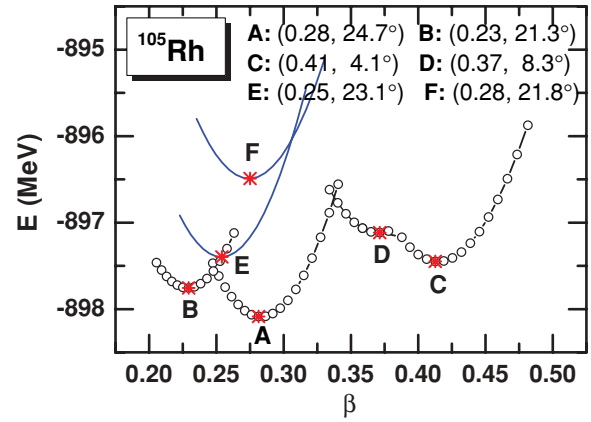

FIG. 2. (Color online) The energy surfaces in adiabatic (open circles) and configuration-fixed (solid lines) constrained triaxial RMF calculations using effective interaction PK1 for ^{105}Rh. The minima in the energy surfaces for the fixed configuration are represented as stars and labeled as A, B, C, D, E, and F. Their corresponding triaxial deformation parameters β and γ are also given.

where $\hat{\mathbf{P}}_{\text{c.m.}}$ is the total momentum operator of a nucleus with mass number A. In order to save time, the constrained triaxial RMF calculations without the time-odd fields are performed to search for the triaxial deformation parameters and the valence nucleons configuration favorable for chirality, which will be later confirmed by the calculations with time-odd fields.

The potential energy surface in the β-γ plane ($0 \leqslant \gamma \leqslant 60^\circ$) for ^{105}Rh in the adiabatic constrained triaxial RMF calculations with PK1 is shown in Fig. 1. All energies are normalized with respect to the binding energy of the absolute minimum, and the contours join points on the surface with the same energy (in MeV). The energy separation between contour lines is 0.4 MeV. Figure 1 shows that the ground state of ^{105}Rh is triaxially deformed with $\beta = 0.28$ and $\gamma = 23^\circ$. The second minimum is located at the area with $\beta \approx 0.4$ and $\gamma \approx 5^\circ$. The energy difference between these two minima is about 0.5 MeV, and the corresponding barrier height is about 1.5 MeV. The behavior of shape coexistence is clearly shown.

The β^2-constrained calculations, in which the triaxial deformation γ is automatically obtained by minimizing the energy, have also been performed. In Fig. 2, the potential energy surfaces as a function of β in adiabatic (open circles) constrained triaxial RMF calculation with PK1 for ^{105}Rh are given, where four minima observed in the potential energy surfaces are labeled with A, B, C, and D.

The total energies E_{tot}, triaxial deformation parameters β and γ, and their corresponding configurations of minima for A–D in the constrained triaxial RMF calculations are presented in Table I. Here, state A represents the ground state, with triaxial deformation $\beta = 0.28$, $\gamma = 24.7^\circ$ and the corresponding valence nucleon configuration $\pi 1g_{9/2}^{-3} \otimes \nu 1h_{11/2}^{2}$. Note that two of the three proton holes in the $1g_{9/2}$ orbital and two neutrons in the $1h_{11/2}$ orbital are pairwise; i.e., they occupy the degenerate time-reversal conjugate levels and do not contribute to the angular momentum. The corresponding unpaired nucleon configuration is $\pi 1g_{9/2}^{-1}$. For state B, the triaxial deformation parameter is $\beta = 0.23$, $\gamma = 21.3^\circ$, with the corresponding valence nucleon configuration $\pi 1g_{9/2}^{-3} \otimes \nu(1g_{7/2}^{-2}2d_{5/2}^{4})$ and unpaired nucleon configuration $\pi 1g_{9/2}^{-1}$. Although A and B have different valence nucleon configurations, they have the same unpaired nucleon configuration.

The triaxial deformation parameters for excited states C and D are $\beta = 0.41$, $\gamma = 8.3^\circ$ and $\beta = 0.37$, $\gamma = 8.3^\circ$, respectively. The valence nucleon configuration for

TABLE I. The total energies E_{tot}, triaxial deformation parameters β and γ, and their corresponding valence nucleon configurations of minima for states A–F in the configuration-fixed constrained triaxial RMF calculations.

State	Configuration		E_{tot}		
	Valence nucleons	Unpaired nucleons	(MeV)	β	γ
A	$\pi 1g_{9/2}^{-3} \otimes \nu 1h_{11/2}^{2}$	$\pi 1g_{9/2}^{-1}$	−898.09	0.28	24.7°
B	$\pi 1g_{9/2}^{-3} \otimes \nu(1g_{7/2}^{-2}2d_{5/2}^{4})$	$\pi 1g_{9/2}^{-1}$	−897.76	0.23	21.3°
C	$\pi(1g_{9/2}^{-4}2p_{3/2}^{-1}1g_{7/2}^{2}) \otimes \nu(1g_{7/2}^{-2}3s_{1/2}^{2}1h_{11/2}^{2})$	$\pi 2p_{3/2}^{-1}$	−897.45	0.41	4.1°
D	$\pi(1g_{9/2}^{-4}1g_{7/2}^{1}) \otimes \nu(1g_{7/2}^{-2}1h_{11/2}^{4})$	$\pi 1g_{7/2}^{1}$	−897.12	0.37	8.3°
E	$\pi 1g_{9/2}^{-3} \otimes \nu(1h_{11/2}^{1}2d_{5/2}^{1})$	$\pi 1g_{9/2}^{-1} \otimes \nu(1h_{11/2}^{1}2d_{5/2}^{1})$	−897.40	0.25	23.1°
F	$\pi 1g_{9/2}^{-3} \otimes \nu(1h_{11/2}^{1}1h_{11/2}^{1})$	$\pi 1g_{9/2}^{-1} \otimes \nu(1h_{11/2}^{1}1h_{11/2}^{1})$	−896.40	0.28	21.8°

C is $\pi(1g_{9/2}^{-4}2p_{3/2}^{-1}1g_{7/2}^{2}) \otimes \nu(1g_{7/2}^{-2}3s_{1/2}^{2}1h_{11/2}^{2})$ and for D is $\pi(1g_{9/2}^{-4}1g_{7/2}^{1}) \otimes \nu(1g_{7/2}^{-2}1h_{11/2}^{4})$, while the unpaired nucleon configuration for C is $\pi 2p_{3/2}^{-1}$ and for D is $\pi 1g_{7/2}^{1}$. The quadrupole deformations of states C and D are larger than for states A and B, which is due to the deformation-driving orbital $\pi 1g_{7/2}$ in states C and D. It should be pointed out that states A, B, C, and D do not have the suitable particle-hole configurations for chirality.

In Refs. [23,24], the observed partner bands with the configurations $\pi 1g_{9/2}^{-1} \otimes \nu 1h_{11/2}^{1}(1g_{7/2}, 2d_{5/2})^{1}$ and $\pi 1g_{9/2}^{-1} \otimes \nu(1h_{11/2}^{1}1h_{11/2}^{1})$ are suggested as candidates for chiral doublet bands. It is interesting to examine the triaxial deformation of these states. For this purpose, the configuration-fixed constrained calculations with the suggested configurations are performed, and their corresponding energy surfaces are given in Fig. 2 as blue solid lines, and the energies, configurations, and triaxial deformation parameters are listed in Table I. The excitation energy for minima E is 0.69 MeV and for F is 1.69 MeV. Furthermore, the triaxial deformation suitable for chirality is found for E and F, namely, 23.1° and 21.8°, respectively, which, together with the corresponding high-j proton-hole and high-j neutron-particle configurations, will lead to the MχD phenomenon [20]. It should be noted that the present RMF calculations are restricted to the nonrotating mean field only, while the TAC calculations with Woods-Saxon potentials have demonstrated that the rotating mean field will become chiral for configuration E at $\hbar\omega = 0.20$ MeV (strong paring) [23] and for configuration F at $\hbar\omega = 0.60$ MeV (zero pairing) or 0.45 MeV (strong paring) [24]. Recently, the doublet bands with configuration F in ^{105}Rh were also investigated by triaxial PRM calculations, and the evolution of the chiral geometry with angular momentum was discussed [31].

The neutron and proton single-particle levels as functions of deformation β are given in Fig. 3, obtained in the adiabatic constrained triaxial RMF calculations for the region $0.247 < \beta < 0.315$. The occupations of neutrons and protons for A, E, and F are given in the top and bottom plots in Fig. 3, respectively. The single-particle levels with positive (negative) parity are marked by solid (dashed) lines, and occupations are represented by filled circles (two particles) and stars (one particle). It should be pointed out that every single-particle level is degenerated with opposite simplex quantum number [19]. It is easy to see that for ground state A, one valence proton occupies the $1g_{9/2}$ orbit, and the last two neutrons occupy the degenerated time-reversal conjugate orbit $1h_{11/2}$. For the positive-parity state F, the two $1h_{11/2}$ neutrons are unpaired (in contrast to state A); i.e., they occupy two different $1h_{11/2}$ levels. For the negative-parity state E, the two unpaired neutrons occupy the $1h_{11/2}$ and $2d_{5/2}$ levels. It is interesting to note that states E and F compete with each other in energy. However, due to different parities, states E and F do not mix and could contribute the MχD phenomenon [20].

As in Ref. [22], the calculations with time-odd fields are also performed to confirm the above discussions. In Table II, the calculated triaxial deformation parameters β and γ, total energies $E_{\rm tot}$, and the excitation energies $E_{\rm x}$ for states E and F with and without time-odd fields are given and compared with the experimental band-head energies of two rotational bands.

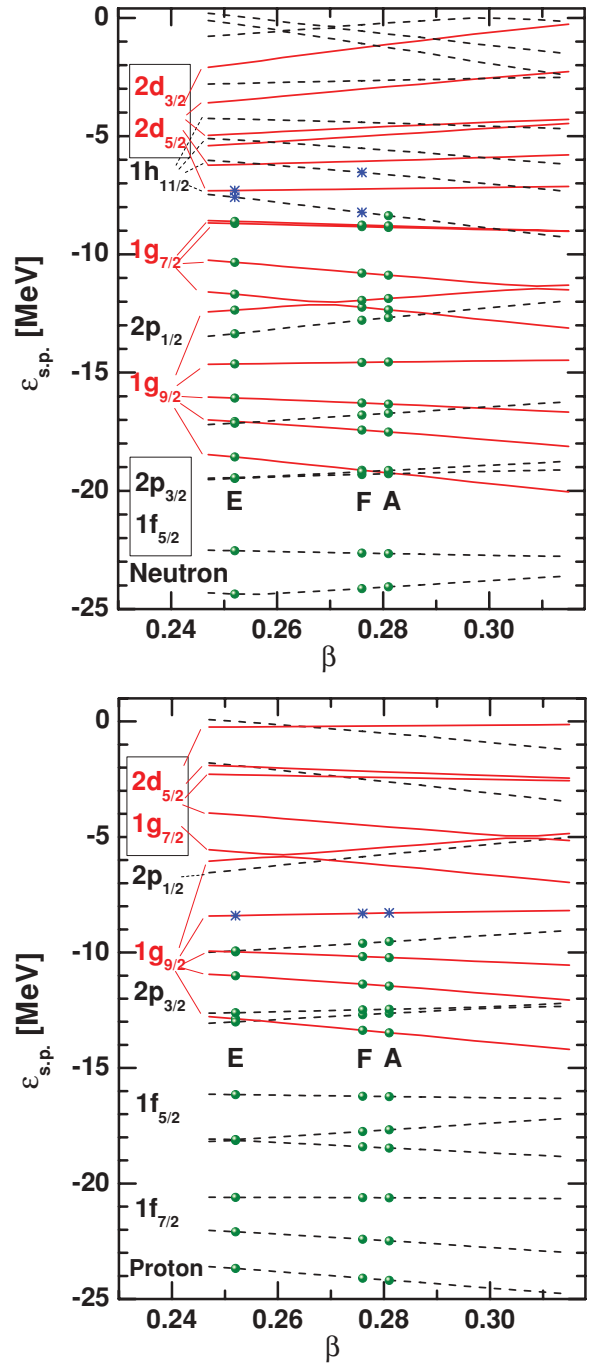

FIG. 3. (Color online) Neutron and proton single-particle levels obtained in constrained triaxial RMF calculations with PK1 as functions of deformation β. Positive (negative) parity states are marked by solid (dashed) lines. Occupations corresponding to the minima in Fig. 2 are represented by filled circles (two particles) and stars (one particle).

The effects of the time-odd fields on the triaxial deformation parameters β and γ are negligible. Their contributions to the total energy are -0.05 MeV for state A, -0.3 MeV for state E, and -0.36 MeV for state F.

The experimental spin, parity, and excitation energies of band heads for two rotational bands based on the

TABLE II. The triaxial deformation parameters β and γ, total energies $E_{\rm tot}$, and the excitation energies $E_{\rm x}$ for states E and F calculated with and without time-odd fields, compared with the experimental band-head energies of two rotational bands based on the configurations of E and F. The spin and parity I^{π} for ground states and band heads of two rotational bands are also given.

State	Time-even fields		Time-odd fields		Experiment	
	(β, γ)	$E_{\rm x}$ ($E_{\rm tot}$) (MeV)	(β, γ)	$E_{\rm x}$ ($E_{\rm tot}$) (MeV)	I^{π}	$E_{\rm x}$
A	(0.28, 24.7°)	(−898.09)	(0.28, 24.9°)	(−898.14)	$\frac{7}{2}^{+}$	
E	(0.25, 23.1°)	0.69 (−897.40)	(0.25, 23.3°)	0.37 (−897.76)	$\frac{15}{2}^{-}$	2.417
F	(0.28, 21.8°)	1.69 (−896.40)	(0.28, 22.1°)	1.43 (−896.70)	$\frac{23}{2}^{+}$	2.982

configurations of E and F are $\frac{15}{2}^{-}$, 2.417 MeV and $\frac{23}{2}^{+}$, 2.982 MeV, respectively. It can be seen that the displacement for the energies of two band heads (0.57 MeV) has been reasonably reproduced by the RMF calculations (1.0 and 1.06 MeV).

It is necessary to note here that in ^{105}Rh, the suggested configuration $\pi 1g_{9/2}^{-1} \otimes \nu 1h_{11/2}^{1}(1g_{7/2}, 2d_{5/2})^{1}$ for the candidate chiral doublet bands (bands 7 and 8 in Ref. [23]) involves the orbits of pseudospin doublet states $(1g_{7/2}, 2d_{5/2})$. So a competing interpretation of bands 7 and 8 includes the pseudospin doublet bands [3]. Further efforts are needed to address this point.

In summary, adiabatic and configuration-fixed constrained triaxial RMF approaches have been applied to investigate the MχD candidate nucleus ^{105}Rh. According to the suggested high-j proton-hole and high-j neutron-particle configurations, their triaxial deformations favorable for the construction of the chiral doublet bands are obtained from the configuration-fixed constrained triaxial RMF calculations. The existence of the MχD phenomenon is expected in ^{105}Rh. Future efforts should be made to investigate whether the rotating mean field will attain chirality or not.

This work is partly supported by Major State Basic Research Developing Program 2007CB815000 and the National Natural Science Foundation of China under Grants No. 10975007, No. 10975008, and No. 110050691.

[1] S. Frauendorf and J. Meng, Nucl. Phys. A **617**, 131 (1997).
[2] K. Starosta *et al.*, Phys. Rev. Lett. **86**, 971 (2001).
[3] J. Meng and S. Q. Zhang, J. Phys. G **37**, 064025 (2010).
[4] J. Meng, S. Q. Zhang, B. Qi, and S. Y. Wang, J. Phys. Conf. Ser. **205**, 012030 (2010).
[5] V. I. Dimitrov, S. Frauendorf, and F. Donau, Phys. Rev. Lett. **84**, 5732 (2000).
[6] P. Olbratowski, J. Dobaczewski, J. Dudek, and W. Plociennik, Phys. Rev. Lett. **93**, 052501 (2004).
[7] P. Olbratowski, J. Dobaczewski, and J. Dudek, Phys. Rev. C **73**, 054308 (2006).
[8] J. Peng, J. Meng, and S. Q. Zhang, Phys. Rev. C **68**, 044324 (2003).
[9] T. Koike, K. Starosta, and I. Hamamoto, Phys. Rev. Lett. **93**, 172502 (2004).
[10] S. Y. Wang, S. Q. Zhang, B. Qi, and J. Meng, Phys. Rev. C **75**, 024309 (2007).
[11] S. Q. Zhang, B. Qi, S. Y. Wang, and J. Meng, Phys. Rev. C **75**, 044307 (2007).
[12] B. Qi *et al.*, Phys. Lett. B **675**, 175 (2009).
[13] P. Ring, Prog. Part. Nucl. Phys. **37**, 193 (1996).
[14] D. Vretenar, A. V. Afanasjev, G. A. Lalazissis, and P. Ring, Phys. Rep. **409**, 101 (2005).
[15] J. Meng *et al.*, Prog. Part. Nucl. Phys. **57**, 470 (2006).
[16] W. Koepf and P. Ring, Nucl. Phys. A **493**, 61 (1989).
[17] A. V. Afanasjev, P. Ring, and J. König, Nucl. Phys. A **676**, 196 (2000).
[18] H. Madokoro, J. Meng, M. Matsuzaki, and S. Yamaji, Phys. Rev. C **62**, 061301 (2000).
[19] J. Peng, J. Meng, P. Ring, and S. Q. Zhang, Phys. Rev. C **78**, 024313 (2008).
[20] J. Meng, J. Peng, S. Q. Zhang, and S.-G. Zhou, Phys. Rev. C **73**, 037303 (2006).
[21] J. Peng *et al.*, Phys. Rev. C **77**, 024309 (2008).
[22] J. M. Yao *et al.*, Phys. Rev. C **79**, 067302 (2009).
[23] J. A. Alcántara-Núñez *et al.*, Phys. Rev. C **69**, 024317 (2004).
[24] J. Timár *et al.*, Phys. Lett. B **598**, 178 (2004).
[25] J. M. Yao, H. Chen, and J. Meng, Phys. Rev. C **74**, 024307 (2006).
[26] J. Li, Y. Zhang, J. M. Yao, and J. Meng, Sci. China, Ser. G **52**, 1586 (2009).
[27] R. Bengtsson and W. Nazarewicz, Z. Phys. A **334**, 269 (1989).
[28] Z. P. Li, T. Nikšić, D. Vretenar, and J. Meng, Phys. Rev. C **81**, 034316 (2010).
[29] W. Long, J. Meng, N. Van Giai, and S.-G. Zhou, Phys. Rev. C **69**, 034319 (2004).
[30] P. Zhao, B. Sun, and J. Meng, Chin. Phys. Lett. **26**, 112102 (2009).
[31] B. Qi, S. Q. Zhang, S. Y. Wang, J. Meng, and T. Koike, Phys. Rev. C 83, 034303 (2011).